Supplemental material to "Aerothermodynamics of a sphere in a monatomic gas based on *ab initio* interatomic potentials over a wide range of gas rarefaction: transonic, supersonic and hypersonic flows."

Felix Sharipov [1]† and Alexey N. Volkov [2]

[1]Departamento de Física, Universidade Federal do Paraná, Caixa Postal 19044, Curitiba 81531-980, Brazil

[2]Department of Mechanical Engineering, University of Alabama, H.M. Comer Hall, 7th Avenue, Tuscaloosa, AL 35487, USA

1. Boundary condition

In the present section, the standard procedure to generate a free stream of particles (Bird 1994, 2013) is described for the problem in question. At the front boundary $x = -R_d$, the particle are generated in the velocity component ranges $0 < v_x < \infty$, $-\infty < v_y < \infty$ and $-\infty < v_z < \infty$. The components v_y and v_z obey the distributions

$$f(v_i) = \frac{1}{\sqrt{\pi}v_\infty}\exp\left(-\frac{v_i^2}{v_\infty^2}\right), \quad i = y, z. \tag{1.1}$$

First, two quantities are generated as

$$v_p = v_\infty\sqrt{-\ln R_f}, \quad \varphi = 2\pi R_f, \tag{1.2}$$

then the components v_y and v_z are calculated by

$$v_y = v_p\cos\varphi, \quad v_z = v_p\sin\varphi. \tag{1.3}$$

Here, R_f are random fractions in the range [0,1]. Note, when a random fraction R_f is generated it is used only once. Another fraction is generated for a next operation. The v_x

† Email address for correspondence: sharipov@fisica.ufpr.br

component obeys the distribution

$$f(v_x) = Av_x \exp\left[-\left(\frac{v_x}{v_\infty} - S\right)^2\right], \quad S = \frac{U_\infty}{v_\infty}, \tag{1.4}$$

where A is the normalization constant which does matter for the generation because we will use only the ratio of $f(v_x)$ to its maximum value

$$\frac{f(v_x)}{\max[f(v_x)]} = \frac{2v_x/v_\infty}{S + \sqrt{S^2+2}} \exp\left[-\left(\frac{v_x}{v_\infty} - S\right)^2 + \frac{1}{4}\left(\sqrt{S^2+2} - S\right)^2\right]. \tag{1.5}$$

In this case, the acceptance-rejection method is used. First, a component values is generated as

$$v_x = v_\infty(10 + S)R_f\,. \tag{1.6}$$

Then the generated value is accepted if the condition

$$\frac{f(v_x)}{\max[f(v_x)]} > R_f \tag{1.7}$$

is true for the generated v_x.

In the rear boundary, $x = R_d$, the procedure is the same with the difference that only negative values of v_x are generated as

$$v_x = -v_\infty(10 - S)R_f\,. \tag{1.8}$$

In the upper boundary, $y = R_d$ and $-R_d \leqslant x \leqslant R_d$, the v_x and v_z components are generated as

$$v_x = v_p \cos\varphi + U_\infty, \quad v_z = v_p \sin\varphi, \tag{1.9}$$

where v_p and φ are generated by (1.2). The component v_y is generated as

$$v_y = v_\infty\sqrt{-\ln R_f}\,. \tag{1.10}$$

2. Numerical error

The coefficients C_D and C_D calculated using several combinations of the parameters Δr, Δt, and R_d are given in Table 1 for $\delta = 0.1$ and in Tables 2 and 3 for $\delta = 10$. These data show the convergence of C_D and C_D within 0.5% when the parameters Δr and Δt decrease and the parameter R_d increases.

To estimate the statistical scattering, let us denote the coefficient calculated in one time

$\frac{R}{\Delta r}$	$\Delta t\frac{v_\infty}{R}$	$Ma=1$ $\frac{R_d}{R}$	C_D	C_Q	$Ma=2$ $\frac{R_d}{R}$	C_D	C_Q	$Ma=5$ $\frac{R_d}{R}$	C_D	C_Q	$Ma=10$ $\frac{R_d}{R}$	C_D	C_Q
40	0.005	4	4.910	0.4527	4	3.021	0.2965	4	2.167	0.2367	4	1.958	0.2252
20	0.002	4	4.905	0.4517	4	3.020	0.2963	4	2.167	0.2367	4	1.957	0.2251
20	0.005	4	4.911	0.4527	4	3.018	0.2961	4	2.168	0.2368	4	1.957	0.2251
20	0.005	8	4.876	0.4497	8	3.003	0.2943	8	2.155	0.2352	6	1.954	0.2246
20	0.005	12	4.882	0.4495	12	2.996	0.2934	12	2.159	0.2356	9	1.954	0.2246

Table 1: Influence of domain size R_d, cell size Δr, and time step Δt on the drag C_D and energy transfer C_Q coefficients for $\delta = 0.1$.

$\Delta t\frac{v_\infty}{R}$	$Ma=1$ $\frac{R_d}{R}$	$\frac{R}{\Delta r}$	C_D	C_Q	$Ma=2$ $\frac{R_d}{R}$	$\frac{R}{\Delta r}$	C_D	C_Q
0.002	10	90	2.024	0.09350	4	90	1.528	0.07667
0.001	10	60	2.025	0.09355	4	60	1.530	0.07699
0.002	10	60	2.024	0.09357	4	60	1.531	0.07696
0.002	20	60	2.061	0.09339	6	60	1.531	0.07705
0.002	30	60	2.064	0.09325				

Table 2: Influence of domain size R_d, cell size Δr, and time step Δt on the drag C_D and energy transfer C_Q coefficients for $\delta = 10$ and $Ma = 1, 2$.

$\Delta t\frac{v_\infty}{R}$	$Ma=5$ $\frac{R_d}{R}$	$\frac{R}{\Delta r}$	C_D	C_Q	$Ma=10$ $\frac{R_d}{R}$	$\frac{R}{\Delta r}$	C_D	C_Q
0.002	4	120	1.239	0.07101	3	240	1.177	0.07049
0.001	4	80	1.242	0.07148	3	160	1.178	0.07042
0.002	4	80	1.243	0.07150	3	160	1.179	0.07069
0.002	6	80	1.242	0.07152	5	160	1.179	0.07070

Table 3: Influence of domain size R_d, cell size Δr, and time step Δt on the drag C_D and energy transfer C_Q coefficients for $\delta = 10$ and $Ma = 5, 10$.

step as C_i. Then its mean value is given as

$$\bar{C} = \frac{1}{N_s}\sum_{i=1}^{N_s} C_i, \tag{2.1}$$

where $N_s \gg 1$ is the number of the time steps. The relative standard error of the mean is given as

$$\sigma = \frac{1}{\bar{C}N_s}\sqrt{\sum_{i=1}^{N_s}\left(C_i - \bar{C}\right)^2} \times 100\%. \tag{2.2}$$

The values of σ for C_D and C_Q are given in Table 4 showing that $\sigma \leqslant 0.1\%$ in all cases.

	$Ma = 1$			$Ma = 2$			$Ma = 5$			$Ma = 10$		
		$\sigma(\%)$			$\sigma(\%)$			$\sigma(\%)$			$\sigma(\%)$	
δ	N_s	C_D	C_Q	N_s	C_D	C_Q	N_s	C_D	C_Q	N_s	C_D	C_Q
0.1	10^5	0.1	0.17	10^5	0.07	0.09	10^4	0.09	0.09	10^4	0.05	0.05
10	10^5	0.04	0.1	$5 \cdot 10^4$	0.03	0.08	10^4	0.03	0.04	10^4	0.08	0.01

Table 4: Relative standard error of the mean σ for the drag C_D and energy transfer C_Q coefficients.

3. Flow field

Two dimensional distributions of density $n(x, r)$, temperature $T(x, r)$ and gas speed $u(x, r)$ are given in Figures1, 2, and 3 for $Ma = 1$, 5, and 10, respectively. The axial distributions of the same quantities for the diffuse and non-diffuse reflections are given in Figure 4. The axial distributions of the same quantities for the cold sphere ($T_w = T_\infty$) and for the hot sphere ($T_w = T_s$) are given in Figure 5. The distribution of the local coefficients C_p and C_h for the cold and hot spheres are given in Figure 6.

4. Comparison with data available in the literature

In Figure 7, the drag coefficient C_D calculated in the present work for ^{4}He at diffuse scattering and $T_w = 300$ K or $T_w = T_s$ is compared with that published in the literature. In addition, the semi-empirical formulas of C_D by Henderson (1976); Loth *et al.* (2021) are also plotted in Figure 7. The conditions for each data set used in the comparison are summarized in Table 5, which shows that the data available in the literature were obtained under conditions different from those used in the present work. Some previously published paper do not provide information necessary to reproduce their results. Therefore, the comparison given in Figure 7 is only qualitative without a deep analysis of discrepancies.

As can be seen, the semi-empirical formulas by Henderson (1976); Loth *et al.* (2021) are in a disagreement between them, but the curve by Loth *et al.* (2021) is closer to the results based on AI potentials. The experimental data by Bailey & Hiatt (1971) are in a reasonable agreement with the present results at the small Mach numbers, i.e. at $Ma = 1$ and 2. At $Ma = 5$, the data by Bailey & Hiatt (1971) have a significant dispersion and discrepancy with the present data. The results by Vogenitz *et al.* (1968) at $T_w = T_s$ fit well our results obtained under the same thermal condition. The data by Dogra *et al.* (1994) are close to our results at $T_w = T_s$. Loth *et al.* (2021) reported just few values of C_D obtained under the condition $T_w = T_\infty$ which are in agreements with the present results corresponding to the same T_w.

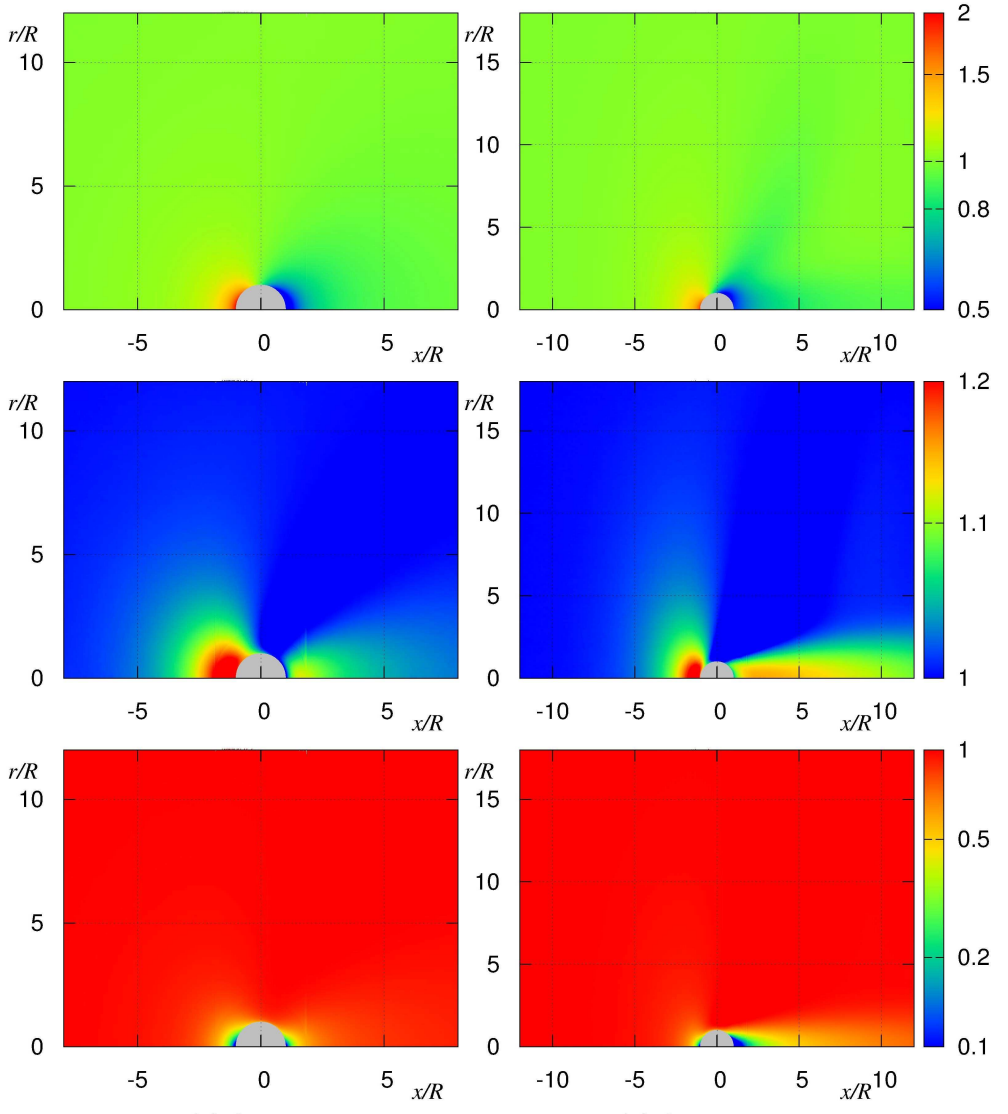

(a) $\delta = 1$ (b) $\delta = 10$

Figure 1: Fields of density n/n_∞, temperature T/T_∞, and speed u/U_∞ of neon at $Ma = 1$, diffuse scattering , $T_\infty = T_w = 300$ K: left - $\delta = 1$; right - $\delta = 10$.

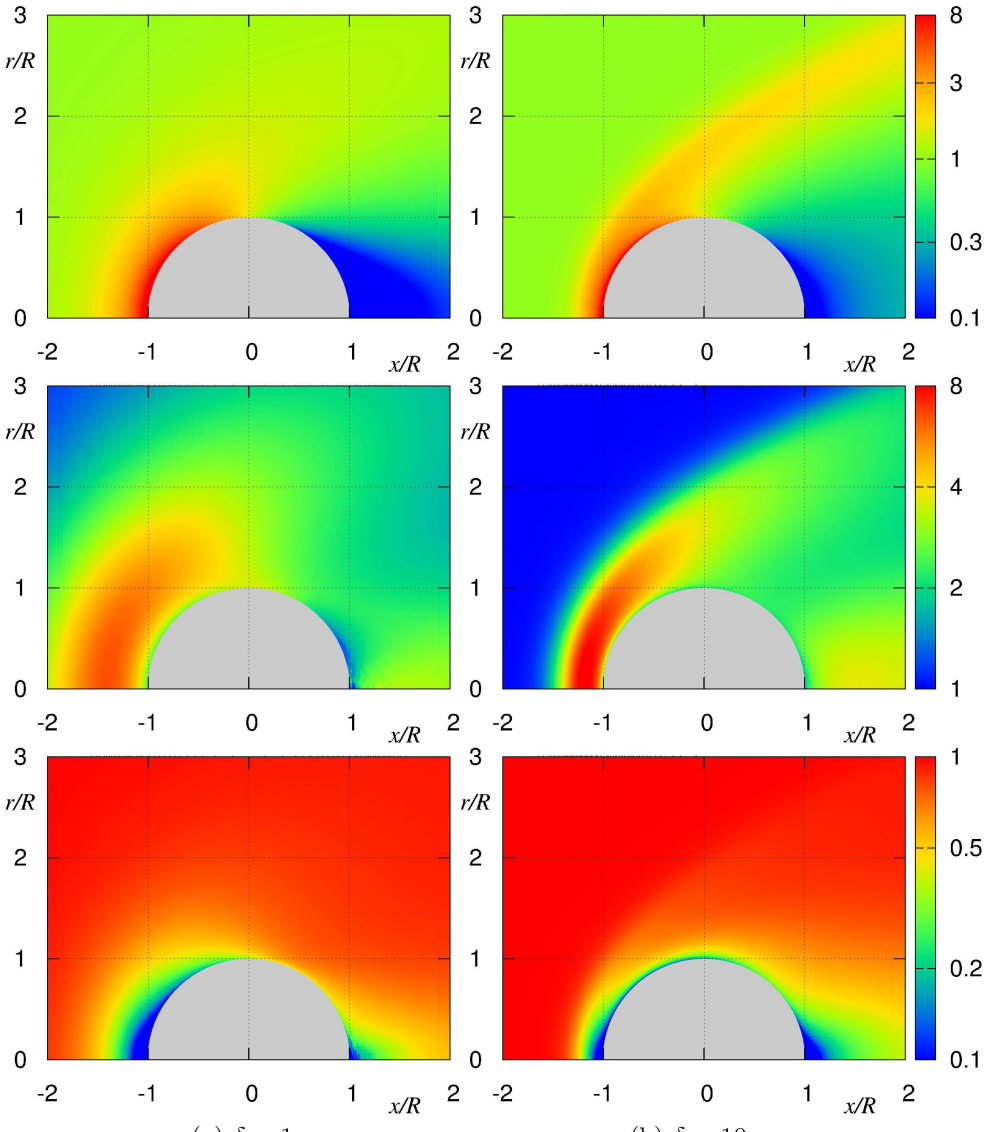

(a) $\delta = 1$ (b) $\delta = 10$

Figure 2: Fields of density n/n_∞, temperature T/T_∞, and speed u/U_∞ of neon at $Ma = 5$, diffuse scattering , $T_\infty = T_w = 300$ K: left - $\delta = 1$; right - $\delta = 10$.

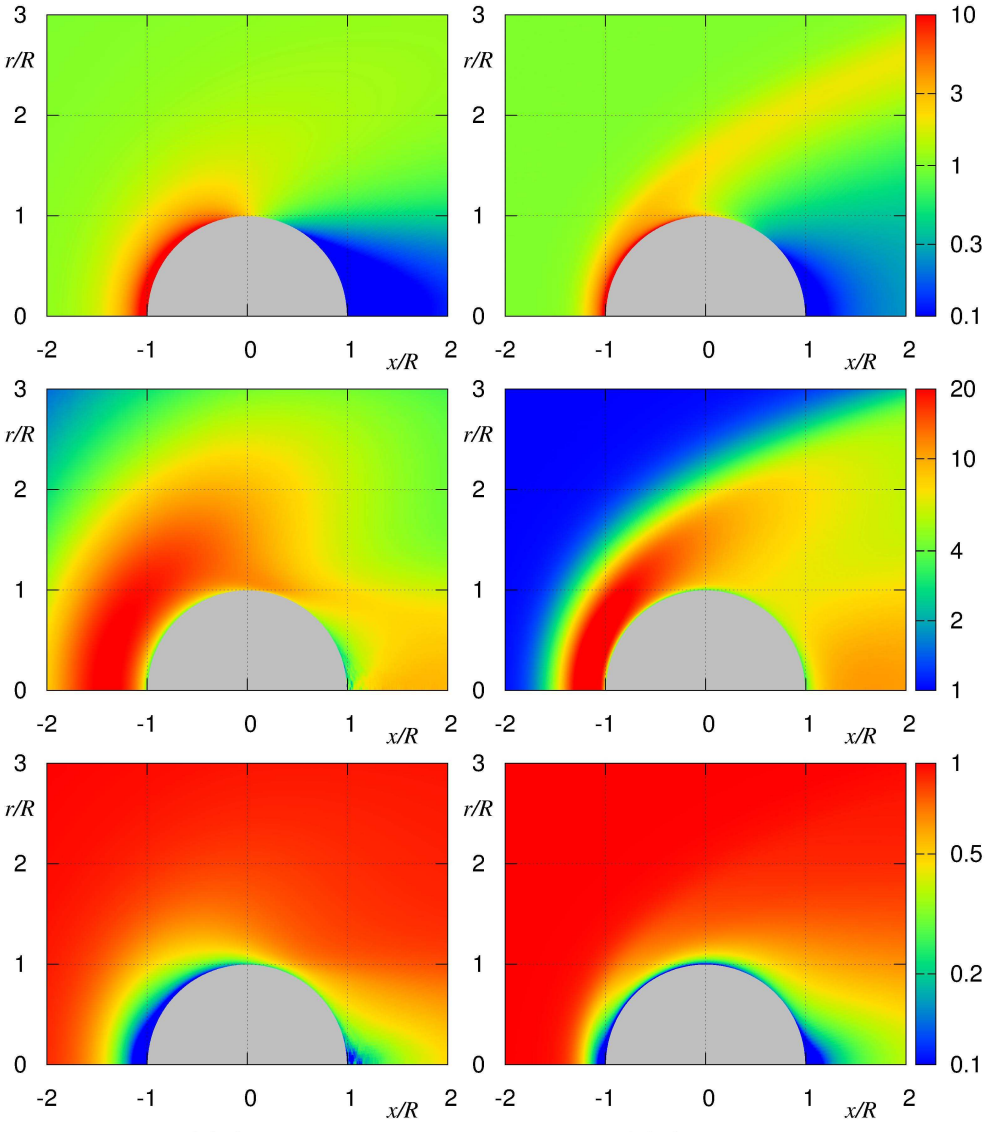

(a) $\delta = 1$ (b) $\delta = 10$

Figure 3: Fields of density n/n_∞, temperature T/T_∞, and speed u/U_∞ of neon at $Ma = 10$, diffuse scattering , $T_\infty = T_w = 300$ K: left - $\delta = 1$; right - $\delta = 10$.

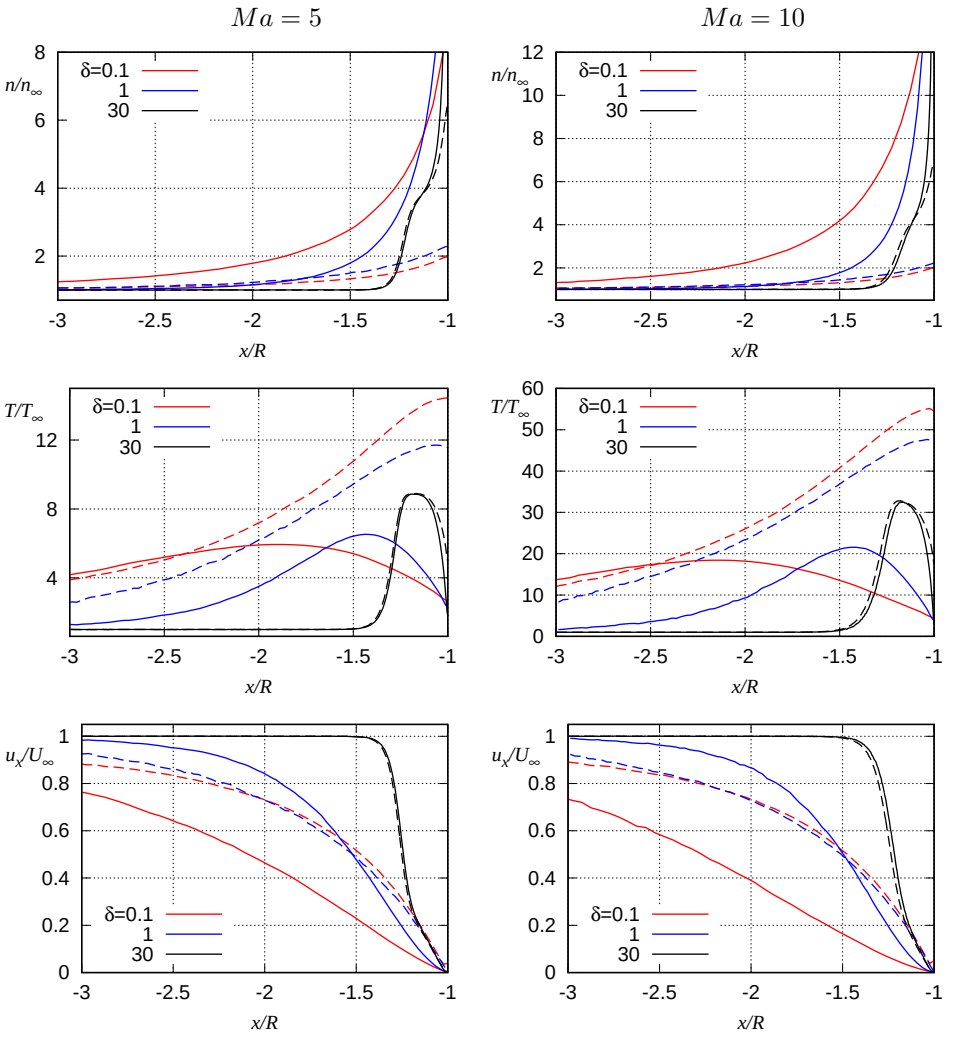

Figure 4: Axial distributions of density n/n_∞, temperature T/T_∞, and velocity u_x/U_∞ at $T_\infty = T_w = 300$ K for ^{4}He: left - $Ma = 5$; right - $Ma = 10$; solid lines - diffuse scattering ; dashed lines - $\alpha_t = 0.4$, $\alpha_n = 0.01$.

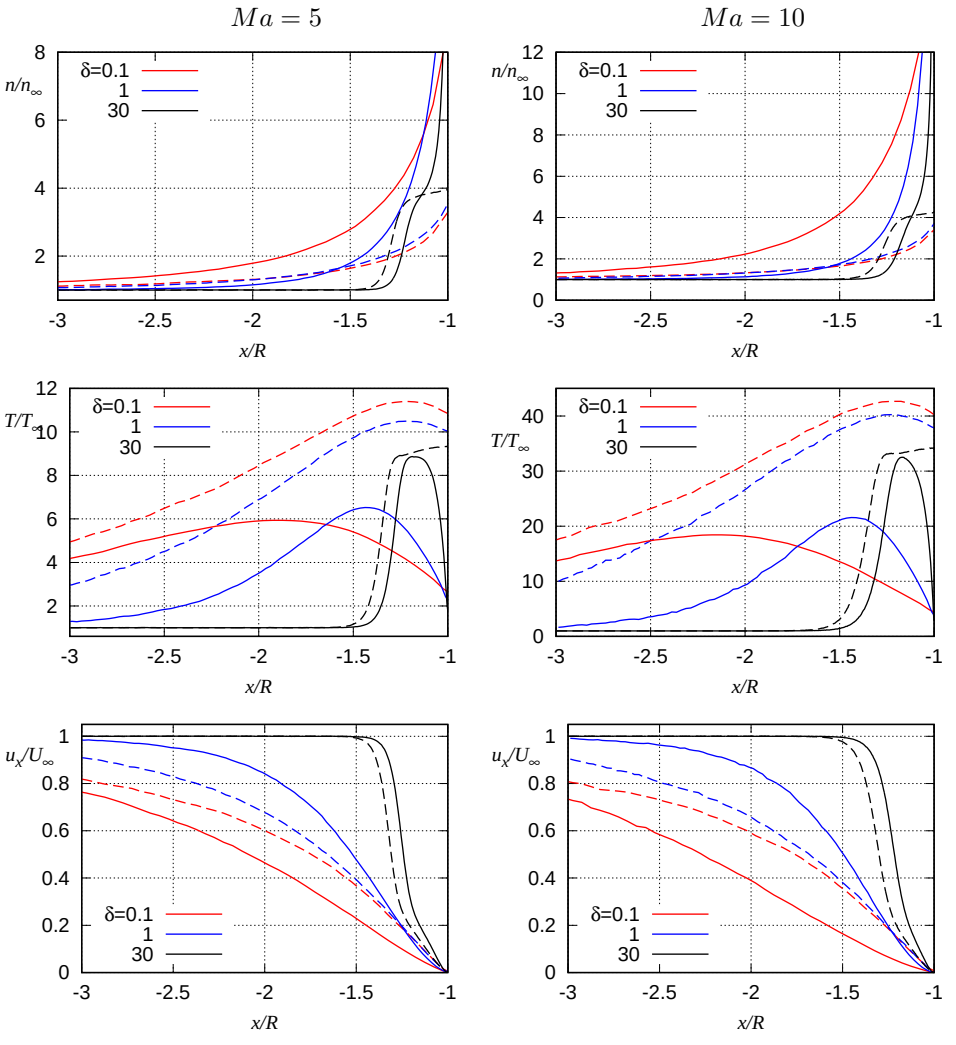

Figure 5: Axial distributions of density n/n_∞, temperature T/T_∞, and velocity u_x/U_∞ at $T_\infty = 300$ K and diffuse scattering : left - $Ma = 5$; right - $Ma = 10$; solid lines - ^{4}He at $T_w = 300$ K; dashed lines - ^{4}He at $T_w = T_s$.

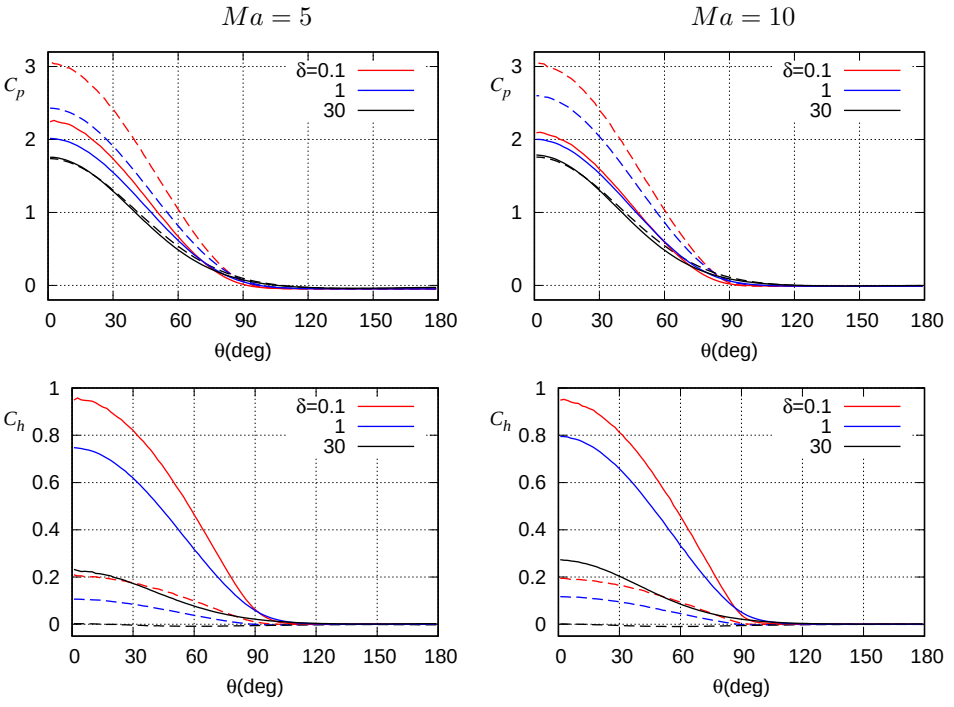

Figure 6: Pressure C_p and energy transfer coefficients C_h vs. angle θ for ^{4}He, diffuse scattering , T_∞ = 300 K: left - Ma = 5; right - Ma = 10; solid lines - T_w = 300 K; dashed lines - $T_w = T_s$.

Ref.	Method	Gas species and molecular model	Gas-surface interaction model	T_∞, T_w
Bailey & Hiatt (1971)	Experiment	air		$T_w = T_\infty$
Vogenitz *et al.* (1968)	2D DSMC	Not specified	diffuse	$T_w = T_\infty$
Dogra *et al.* (1994)	2D DSMC	air, VHS	diffuse	$T_\infty \approx 20$ K, $T_w = 600$ K
Volkov (2011)	3D DSMC	HS	diffuse	$T_w = T_\infty$
Loth *et al.* (2021)	2D DSMC	Not specified	diffuse-specular ($\alpha = 0.9$)	$T_w = T_\infty$

Table 5: Experimental and simulation conditions for the data sets compared in Figure 7. Here, T_∞ is the free stream temperature, T_w is the sphere surface temperature.

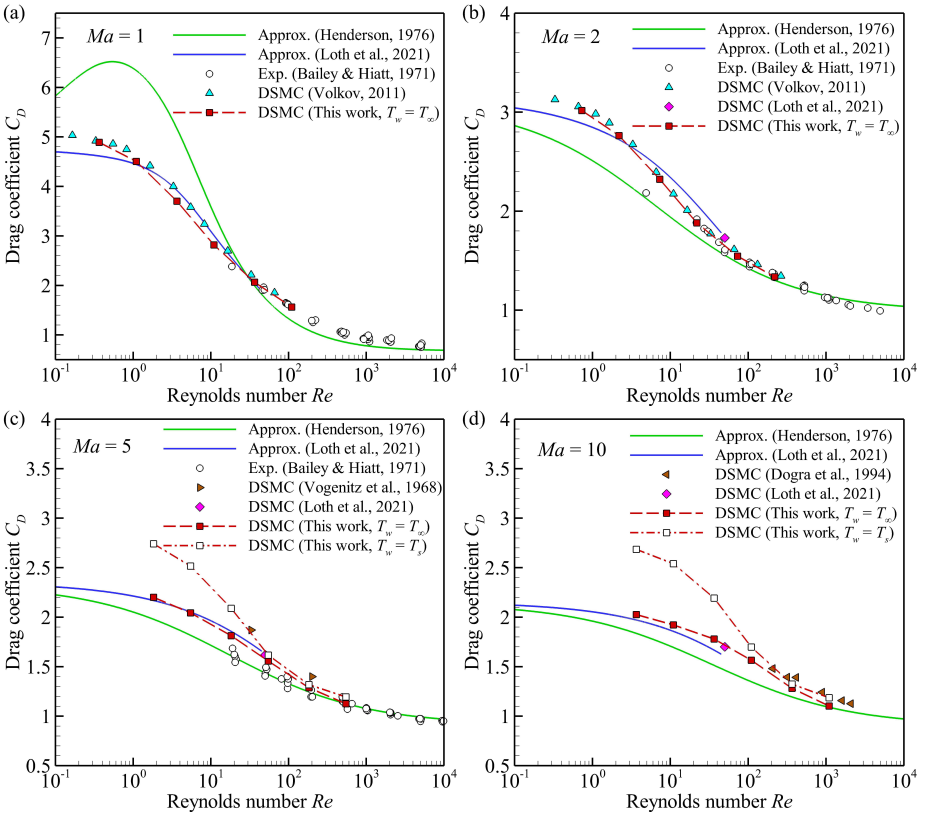

Figure 7: Comparison of drag coefficient C_D obtained in the present work for ^{4}He at diffuse scattering with that obtained by Bailey & Hiatt (1971); Vogenitz *et al.* (1968); Dogra *et al.* (1994); Volkov (2011); Loth *et al.* (2021). The solid curves represent the semi-empirical equations at $T_w = T_\infty$ by Henderson (1976); Loth *et al.* (2021).

REFERENCES

Bailey, A B & Hiatt, J 1971 Free-flight measurements of sphere drag at subsonic, transonic, supersonic, and hypersonic speeds for continuum, transition, and near-free-molecular flow conditions. *Tech. Rep.* AEDC-TR-70-291. Arnold Engineering Development Center report.

Bird, G A 1994 *Molecular Gas Dynamics and the Direct Simulation of Gas Flows*. Oxford: Oxford University Press.

Bird, G A 2013 *The DSMC method*.

Dogra, V K, Moss, J N, Wilmoth, R G & Price, J M 1994 Hypersonic rarefied flow past spheres including wake structure. *J. Spacecraft Rockets* **31** (5), 713–718.

Henderson, C B 1976 Drag coefficients of spheres in continuum and rarefied flows. *AIAA Journal* **14** (6), 707–708.

Loth, E, Tyler Daspit, J, Jeong, M, Nagata, T & Nonomura, T 2021 Supersonic and hypersonic drag coefficients for a sphere. *AIAA Journal* **59** (8), 3261–3274.

Vogenitz, F W, Bird, G A, Broadwell, J E & Rungaldi, H 1968 Theoretical and experimental study of rarefied supersonic flows about several simple shapes. *AIAA J.* **6** (12), 2388–2394.

Volkov, A N 2011 Transitional flow of a rarefied gas over a spinning sphere. *J. Fluid Mech* **683**, 320–345.